Computer Aided Geometric Design 46 (2016) 92–102

Contents lists available at ScienceDirect

Computer Aided Geometric Design

www.elsevier.com/locate/cagd

Medial axis transforms yielding rational envelopes ☆

Michal Bizzarri [a], Miroslav Lávička [b,a], Jiří Kosinka [c,*]

[a] NTIS – New Technologies for the Information Society, University of West Bohemia, Univerzitní 8, 306 14 Plzeň, Czech Republic
[b] Department of Mathematics, University of West Bohemia, Univerzitní 8, 306 14 Plzeň, Czech Republic
[c] Johann Bernoulli Institute, University of Groningen, Nijenborgh 9, 9747 AG Groningen, The Netherlands

ARTICLE INFO

Article history:
Received 29 October 2015
Received in revised form 6 May 2016
Accepted 7 May 2016
Available online 11 May 2016

Keywords:
Rational envelope
Pythagorean hodograph curve
Medial axis
MOS surface

ABSTRACT

Minkowski Pythagorean hodograph (MPH) curves provide a means for representing domains with rational boundaries via the medial axis transform. Based on the observation that MPH curves are not the only curves that yield rational envelopes, we define and study rational envelope (RE) curves that generalise MPH curves while maintaining the rationality of their associated envelopes.

To demonstrate the utility of RE curves, we design a simple interpolation algorithm using RE curves, which is in turn used to produce rational surface blends between canal surfaces. Additionally, we initiate the study of rational envelope surfaces as a surface analogy to RE curves.

1. Introduction

Rational curves and surfaces play a key role in computer aided design (Piegl and Tiller, 1997). However, the important operation of offsetting can produce objects outside this class, even when applied to shapes with rational parametrisations. One way to overcome this limitation is to restrict oneself to a subclass of rational shapes which is closed under offsetting. This led, in the curve case, to the definition of PH curves, i.e., curves with Pythagorean hodographs (Farouki, 2008; Kosinka and Lávička, 2010). A PH curve $\mathbf{x}(t)$ is distinguished by the PH condition $\|\mathbf{x}'(t)\|^2 = \sigma(t)^2$, where $\sigma(t) \in \mathbb{R}(t)$. These curves were introduced as planar polynomial objects. Later, the PH concept was generalised to their rational counterparts by Pottmann (1995).

A closely related issue is that of reconstructing a planar domain's boundary from its medial axis transform (MAT) (Blum, 1967). Similarly to PH curves, only a subclass of rationally parametrised MATs, called Minkowski PH curves, or MPH curves (Moon, 1999; Kosinka and Lávička, 2010), leads to rational domain boundaries. MPH curves are rational curves $(\mathbf{y}(t), r(t))$ in 3-space whose hodographs satisfy the PH condition with respect to the Minkowski inner product with signature $(+,+,-)$.

In this paper, we return to this thoroughly studied problem of MPH and envelope curves (Choi et al., 1999; Kosinka and Jüttler, 2006; Kosinka and Jüttler, 2009; Kosinka and Šír, 2010; Kosinka and Lávička, 2011). As we will see shortly in Section 2, it turns out that if one allows a square-root term (Abhyankar, 1994) in the MAT's representation, a broader class of MATs corresponding to rational envelopes of the associated family of circles is obtained. We call this class rational envelope curves, or RE curves for short.

☆ This paper has been recommended for acceptance by Rida Farouki.

* Corresponding author.
E-mail addresses: bizzarri@ntis.zcu.cz (M. Bizzarri), lavicka@kma.zcu.cz (M. Lávička), j.kosinka@rug.nl (J. Kosinka).

http://dx.doi.org/10.1016/j.cagd.2016.05.006
0167-8396/

Consider a parametric curve $\overline{\mathbf{y}}(t) = (\mathbf{y}(t), r(t))$ in the Minkowski 3-space $\mathbb{R}^{2,1}$ considered as the MAT of its associated domain. The corresponding two branches $\mathbf{x}^{\pm}(t)$ of the envelope curve $\mathbf{x}(t)$ can be parametrised by

$$\mathbf{x}^{\pm}(t) = \mathbf{y}(t) - r(t)\frac{r'(t)\,\mathbf{y}'(t) \pm \mathbf{y}'^{\perp}(t)\sqrt{\|\mathbf{y}'(t)\|^2 - r'^2(t)}}{\|\mathbf{y}'(t)\|^2}, \tag{1}$$

where $\mathbf{x}^{\perp} = (x_2, -x_1)$ for $\mathbf{x} = (x_1, x_2)$. Clearly, an MPH curve, which satisfies

$$\|\mathbf{y}'(t)\|^2 - r'^2(t) = \sigma^2(t) \tag{2}$$

for some rational function $\sigma(t)$, guarantees the rationality of the associated envelope branches $\mathbf{x}^{\pm}$. It was observed in Kosinka and Lávička (2010) that for any MPH curve $\overline{\mathbf{y}}(t) \subset \mathbb{R}^{2,1}$, the associated curves $\mathbf{x}^{\pm} \subset \mathbb{R}^2$ are rational PH curves. Based on this, it was shown that any rational MPH curve $\overline{\mathbf{y}}$ in $\mathbb{R}^{2,1}$ can be constructed starting from a planar rational PH curve $\mathbf{x}$ in $\mathbb{R}^2$ and a rational function r in the form

$$\mathbf{y}(t) = (x_1 + rn_1, x_2 + rn_2, r), \tag{3}$$

where $\mathbf{n} = (n_1, n_2)$ is the rational unit normal vector field associated with $\mathbf{x}$. Building on (3), one can obtain an expression for all rational MPH curves (Kosinka and Lávička, 2010).

The discussion of the interplay between spatial MPH curves and their associated planar PH curves from the point of view of Hermite interpolation was further developed by Kosinka and Lávička (2011). The main advantage of the method presented in Kosinka and Lávička (2011) lies in the fact that it uses, only after some simple additional computations, an arbitrary algorithm for interpolation by planar PH curves also for interpolation by spatial MPH curves. Thus, compared to other MPH schemes, it does not require the complicated Clifford algebra machinery (Choi et al., 2002). We will show in Section 3 that this procedure can be simplified further still with the help of RE curves.

A condition guaranteeing the rationality of contour curves on canal surfaces, which can be used for obtaining rational parametrisations of canal surfaces, was studied by Bizzarri and Lávička (2013). This approach extended the results on rational MPH curves from Kosinka and Lávička (2010) and led to a simple method for computing rational offset blends between two canal surfaces (Bizzarri and Lávička, 2013). We will discuss a similar approach to blending from the point of view of RE curves in Section 4.

A generalisation of PH curves to the surface case led to the class of PN surfaces, i.e., surfaces with Pythagorean normals (Pottmann, 1995). PN surfaces are rational surfaces with rational offsets. Similarly, MOS surfaces, i.e., medial surfaces obeying a certain sum of squares condition (Kosinka and Jüttler, 2007), represent a generalisation of MPH curves to the bivariate setting in $\mathbb{R}^{3,1}$. MOS surfaces correspond to associated domain boundaries which are rational via the envelope formula for medial surface transforms. In this regard, we extend the concept of MOS surfaces to RE surfaces and lay down their basic structure in Section 5. The paper is concluded in Section 6.

2. Rational envelope curves

Turning back to the envelope formula (1), observe that if we start with two rational boundary curves (or envelopes) $\mathbf{x}_{1,2}(t)$ that correspond in parameter, we obtain a rational medial axis. But the full MAT contains, in general, a square-root term in its third coordinate function. Thence, the class of curves in $\mathbb{R}^{2,1}$ that yield rational envelopes must be broader than only the class of rational MPH curves. Indeed, it also comprises curves that can be parametrised by square-roots, which are known to be rational, elliptic, or hyper-elliptic (Abhyankar, 1994; Hartshorne, 1977).

Therefore, we will deal with curves in $\mathbb{R}^{2,1}$ given by $\overline{\mathbf{y}}(t) = \left(\mathbf{y}(t), \sqrt{R(t)}\right)$. This leads to the following envelope formula:

Lemma 2.1. *Let $\overline{\mathbf{y}}(t) = \left(\mathbf{y}(t), \sqrt{R(t)}\right)$ be a regular C^1 parametric curve considered as the MAT of a planar domain with $\mathbf{y}(t)$ and $R(t)$ rational. Then the corresponding envelope is given by*

$$\mathbf{x}^{\pm}(t) = \mathbf{y}(t) - \frac{R'(t)\,\mathbf{y}'(t) \pm \mathbf{y}'^{\perp}(t)\sqrt{4R(t)\|\mathbf{y}'(t)\|^2 - R'^2(t)}}{2\|\mathbf{y}'(t)\|^2}. \tag{4}$$

Additionally, the envelope $\mathbf{x}^{\pm}(t)$ of $\overline{\mathbf{y}}(t)$ is rational if and only if there exists a rational function $\sigma(t)$ such that

$$4R(t)\|\mathbf{y}'(t)\|^2 - R'^2(t) = \sigma^2(t). \tag{5}$$

This lemma gives rise to

Definition 2.2. A parametric curve $\overline{\mathbf{y}}(t) = \left(\mathbf{y}(t), \sqrt{R(t)}\right)$ in $\mathbb{R}^{2,1}$ is called an *RE curve*, i.e., a *curve yielding a Rational Envelope*, if there exists a rational function $\sigma(t)$ such that condition (5) is satisfied.

Clearly, rational MPH curves (including the subclass of polynomial MPH curves) form a proper subset of RE curves.

As mentioned above, any MPH curve can be obtained by using the fact that if $\overline{\mathbf{y}}$ is an MPH curve, its envelopes $\mathbf{x}^{\pm}(t)$ are planar rational PH curves (Kosinka and Lávička, 2010). We now show that an analogous construction is possible in the case of RE curves as well.

First, for a given rational planar curve $\mathbf{x}(t)$, we construct its *one-sided* generalised offset curve $\mathbf{y}(t)$ with varying distance $r(t)$, i.e., the curve in the form

$$\mathbf{y}(t) = \mathbf{x}(t) + r(t)\frac{\mathbf{x}'^{\perp}(t)}{\|\mathbf{x}'(t)\|}. \tag{6}$$

This curve is rational if and only if

$$\frac{r(t)}{\|\mathbf{x}'(t)\|} = f(t) \tag{7}$$

is a rational function. Using (7), we arrive at the class of curves in the form

$$\overline{\mathbf{y}}(t) = \left(x_1 + x_2' f, x_2 - x_1' f, f\sqrt{(x_1')^2 + (x_2')^2}\right). \tag{8}$$

Hence we can formulate the following

Theorem 2.3. *Any RE curve in $\mathbb{R}^{2,1}$ can be expressed in the form of (8). In particular, if $\mathbf{x}(t)$ is a rational PH curve, then (8) describes a rational MPH curve, and any MPH curve can be obtained this way.*

Proof. Substituting (8) into (1) gives the condition $\sigma^2 = \left[2f\left((x_1')^2 + (x_2')^2 + f(x_2'x_1'' - x_1'x_2'')\right)\right]^2$, and thus any curve given by (8) is an RE curve. On the other hand, let us consider an RE curve $\overline{\mathbf{y}}(t) = \left(\mathbf{y}, \sqrt{R}\right)$. Then by definition, there exist two conjugate rational envelope curves $\mathbf{x}^{\pm}(t)$, and since the medial axis $\mathbf{y}(t)$ is rational, the function $f(t) = \sqrt{R}/\|\mathbf{x}'(t)\|$ has to be rational as well. Thus, by setting e.g. $\mathbf{x}(t) = \mathbf{x}^{+}(t)$ and $f(t) = \sqrt{R}/\|\mathbf{x}'(t)\|$ we can construct any RE curve $\overline{\mathbf{y}}(t)$ in the required form of (8). The case when $\mathbf{x}(t)$ is a rational PH curve was proved already in Kosinka and Lávička (2010). □

Additionally, (8) leads to a classification of RE curves in the following form.

Proposition 2.4. *A curve $\overline{\mathbf{y}}(t) = \left(y_1(t), y_2(t), \sqrt{R(t)}\right) \in \mathbb{R}^{2,1}$ is an RE curve if and only if there exist five polynomials $a, b, c, g, h \in \mathbb{R}[t]$ satisfying $\gcd(a, c) = \gcd(b, c) = \gcd(g, h) = 1$ such that*

$$\begin{aligned} y_1(t) &= a/c + (b/c)'g/h, \\ y_2(t) &= b/c - (a/c)'g/h, \\ R(t) &= \left((a/c)'^2 + (b/c)'^2\right)(g/h)^2. \end{aligned} \tag{9}$$

Proof. Consider an MAT defined by (9). A direct computation leads to

$$\sigma(t) = 2g/h\left((a/c)'^2 + (b/c)'^2 + g/h\big((a/c)'(b/c)'' - (a/c)''(b/c)'\big)\right).$$

Hence the corresponding envelope curve is rational. On the other hand, any planar rational curve can be parametrised as $\mathbf{x} = (a/c, b/c)$ and any rational function is given by $f = g/h$. Substitution into (8) gives the formulas in (9). □

Note that for some choices of the polynomials in (9), the resulting $\overline{\mathbf{y}}(t)$ may not be a curve in the strict sense of differential geometry (although it still formally satisfies the RE condition). We do not pursue these technical considerations further. Additionally, the *parameter speed* of $\overline{\mathbf{y}}(t)$ is given by $|\sigma(t)|$.

Building on (9), let a, b, c, g, h be polynomials of degrees d_a, d_b, d_c, d_g, d_h, respectively. Then the rational degree of (9) is given by:

$$\begin{aligned} \deg(\mathbf{y}) &= [\max(d_a, d_b) + d_c + \max(d_h, d_g - 1), 2d_c + d_h], \\ \deg(R) &= [2(\max(d_a, d_b) + d_c + d_g - 1), 2(2d_c + d_h)]. \end{aligned} \tag{10}$$

As we will see below, a prominent subset of the class of RE curves is formed by those for which $\mathbf{x}(t)$ and $f(t)$ are polynomial. In this case, $c(t)$ is constant and $h(t)$ has to divide $a'(t)$ and $b'(t)$. It follows that there exist polynomials $k(t)$

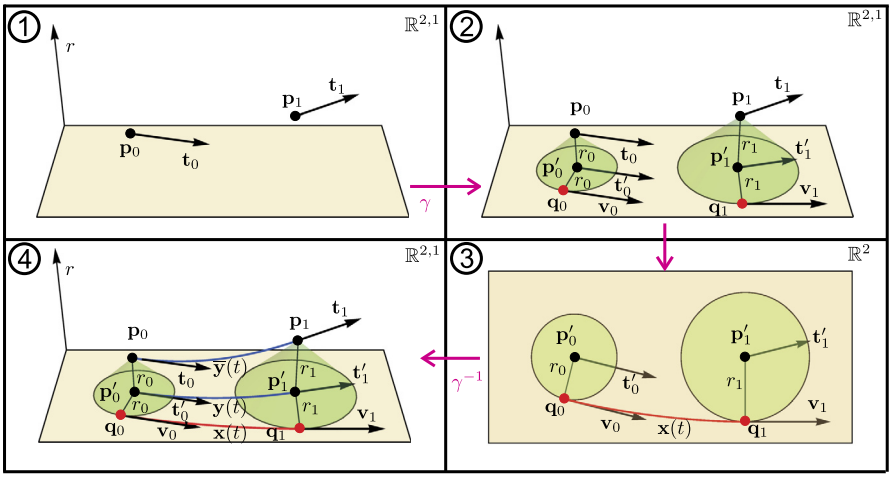

Fig. 1. Our 4-step algorithm for interpolating G^1 data in $\mathbb{R}^{2,1}$ by an RE curve.

and $l(t)$ such that $a'(t) = k(t)h(t)$ and $b'(t) = l(t)h(t)$. Combining this with (9), we obtain

$$\begin{aligned} y_1(t) &= \int k(t)h(t)\mathrm{d}t + l(t)g(t), \\ y_2(t) &= \int l(t)h(t)\mathrm{d}t - k(t)g(t), \\ R(t) &= \left(k(t)^2 + l(t)^2\right) g(t)^2 \end{aligned} \tag{11}$$

with polynomials $k(t)$, $l(t)$, $g(t)$, $h(t)$.

3. Interpolation by RE curves

In Kosinka and Lávička (2011), an interpolation method using MPH splines based on planar PH splines was introduced and thoroughly investigated. While conceptually simpler than previous methods, it still relies on the construction of a PH curve interpolating certain derived data in the plane. This in some situations means that the interpolant does not exist as a single MPH arc, and several arc need to be employed. We now show that if MPH curves are replaced by RE curves, the associated PH interpolation can be replaced by an arbitrary interpolation technique formulated for polynomial or rational planar curves. This guarantees that an RE interpolant always exists. The method is then utilised in Section 4 for constructing rational blending surfaces between two canal surfaces.

As an example, we propose a simple method for interpolating G^1 Hermite data in $\mathbb{R}^{2,1}$ by RE curves. As in Kosinka and Lávička (2011), this method is based on projecting these data to the plane, performing some suitable interpolation in $\mathbb{R}^2$, and finally lifting the interpolant back to $\mathbb{R}^{2,1}$. The whole process consists of 4 steps and is illustrated in Fig. 1.

Consider the following G^1 Hermite input data in $\mathbb{R}^{2,1}$: $\mathbf{p}_i$ (end points) and $\mathbf{t}_i$ (end tangent vectors); $i \in \{0, 1\}$; see Fig. 1, Step 1. Using (1), we obtain the associated points $\mathbf{q}_i \in \mathbb{R}^2$ on the corresponding envelope curve as

$$\mathbf{q}_i = \overset{\triangledown}{\mathbf{p}}_i - p_{i3}\frac{t_{i3}\overset{\triangledown}{\mathbf{t}}_i + \overset{\triangledown}{\mathbf{t}}_i^{\perp}\sqrt{\|\overset{\triangledown}{\mathbf{t}}_i\|^2 - (t_{i3})^2}}{\|\overset{\triangledown}{\mathbf{t}}_i\|^2}, \tag{12}$$

where $\overset{\triangledown}{\mathbf{x}} = (x_1, x_2)$ for $\mathbf{x} = (x_1, x_2, x_3)$; see Fig. 1, Step 2. We choose $\mathbf{v}_i$ as the perpendicular vectors to the vectors $\overset{\triangledown}{\mathbf{p}}_i - \mathbf{q}_i$:

$$\mathbf{v}_i = \alpha_i \frac{\left(\overset{\triangledown}{\mathbf{p}}_i - \mathbf{q}_i\right)^{\perp}}{\|\overset{\triangledown}{\mathbf{p}}_i - \mathbf{q}_i\|}. \tag{13}$$

The magnitudes α_i of $\mathbf{v}_i$ are free parameters and can be chosen to modify the resulting shape. We address this in more detail in our examples below.

In Step 3, we interpolate $\mathbf{q}_i$ and $\mathbf{v}_i$ in the plane by a suitable Hermite interpolation method (we use the Ferguson cubic) and obtain a planar curve $\mathbf{x}(t)$, $t \in [0, 1]$ satisfying

$$\mathbf{x}(i) = \mathbf{q}_i, \quad \text{and} \quad \mathbf{x}'(i) = \mathbf{v}_i, \quad i \in \{0, 1\}. \tag{14}$$

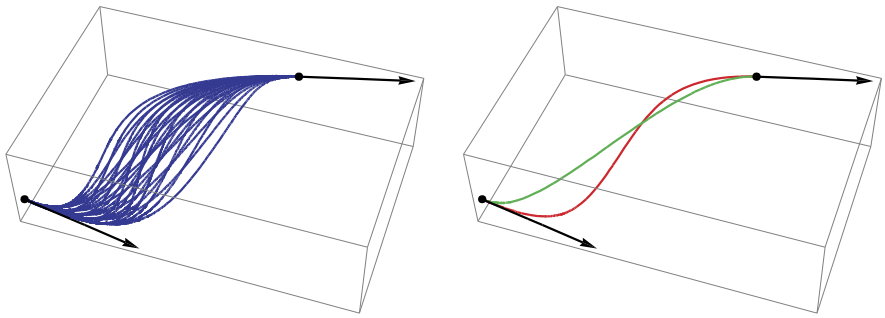

Fig. 2. RE interpolants for the input data (black) from Example 3.2. Left: The two-parametric family of RE interpolants (blue). Right: The RE interpolants with minimal arc-length (green) and minimal elastic bending energy (red). (For interpretation of the references to colour in this figure legend, the reader is referred to the web version of this article.)

Finally, in Step 4, we lift the interpolant $\mathbf{x}(t)$ from $\mathbb{R}^2$ to $\mathbb{R}^{2,1}$. This is done by computing a polynomial $f(t)$ such that the curve

$$\overline{\mathbf{y}}(t) = \left(x_1 + x_2' f, x_2 - x_1' f, f\sqrt{(x_1')^2 + (x_2')^2} \right) \tag{15}$$

interpolates the input data in $\mathbb{R}^{2,1}$. We employ the Ferguson interpolant again, this time given by the Hermite data f_0, f_1, f_0', f_1', where

$$f_i = f(i) = \frac{\mathbf{p}_{i3}}{\|\mathbf{v}_i\|} \quad \text{and} \quad f_i' = f'(i) = -\frac{\overset{\triangledown}{\mathbf{t}}_i \cdot \left(f_i \mathbf{x}''(i) - \mathbf{v}_i^{\perp} \right)}{\overset{\triangledown}{\mathbf{t}}_i \cdot \mathbf{v}_i} \tag{16}$$

were computed by solving

$$\overline{\mathbf{y}}(i) = \mathbf{p}_i \quad \text{and} \quad \overline{\mathbf{y}}'(i) = \beta_i \mathbf{t}_i, \tag{17}$$

where

$$\beta_i = \frac{\mathbf{v}_i \cdot \mathbf{v}_i - f_i \mathbf{x}''(i) \cdot \mathbf{v}_i^{\perp}}{\overset{\triangledown}{\mathbf{t}}_i \cdot \mathbf{v}_i}. \tag{18}$$

This gives the sought-after RE interpolant $\overline{\mathbf{y}}(t)$.

Remark 3.1. To obtain a real envelope, the medial axis transform must be a space-like curve fulfilling the condition $\|\mathbf{y}'(t)\|^2 - r'^2(t) > 0$. In the case of RE curves, this condition reads $4R(t)\|\mathbf{y}'(t)\|^2 - R'^2(t) > 0$. However, as we construct RE curves from one real branch, the reality of the second branch and thus of the whole envelope is automatically guaranteed. So the only condition is that the tangent vectors (as input data for the Hermite interpolation) are space-like, i.e., their angle with the xy-plane is less than $\pi/4$; see Kosinka and Lávička (2011) for more details about the validity conditions of envelopes. We have not encountered a violation of these conditions in any of our examples and tests.

Example 3.2. We construct a family of RE curves interpolating the data

$$\mathbf{p}_0 = (0, 0, 1), \quad \mathbf{p}_1 = (12, 12, 3), \quad \mathbf{t}_0 = (20, 0, -5), \quad \mathbf{t}_1 = (20, 0, 5). \tag{19}$$

The magnitudes α_i of $\mathbf{v}_i$ are free parameters; see (13). The resulting two-parametric set $\mathbf{f}(t, \alpha_0, \alpha_1)$ of solutions is shown in Fig. 2, left. Within this family, we choose suitable interpolants according to two natural criteria (Farouki, 1996, 2002). The first criterion is minimal *arc-length*, i.e., we minimise the following objective function

$$\Phi(\alpha_0, \alpha_1) = \int_0^1 \sqrt{\mathbf{f}(t, \alpha_0, \alpha_1) \cdot \mathbf{f}(t, \alpha_0, \alpha_1)}\, \mathrm{d}t. \tag{20}$$

And the second criterion is minimal *elastic bending energy*, i.e., we minimise

$$\Psi(\alpha_0, \alpha_1) = \int_0^1 \kappa^2(t, \alpha_0, \alpha_1)\, \mathrm{d}t, \tag{21}$$

where κ is the curvature of $\mathbf{f}$. The interpolants with minimal arc-length and minimal elastic bending energy are shown in Fig. 2, right.

Remark 3.3. As was mentioned above, an RE interpolant to G^1 data always exists. This is in contrast to the method used by Kosinka and Lávička (2011), based on planar cubic PH interpolants, where existence of a single MPH interpolating arc is not guaranteed and several concatenated arcs may need to be employed, depending on the mutual position of the input data.

If offsets of the corresponding envelopes are to be rational, MPH curves have to be employed. On the other hand, if the application is aimed at canal surface blending (addressed in the following section), the MPH interpolant can be replaced by the simpler-to-compute RE interpolant.

In summary, the situation is not as clear-cut as it may seem at first sight. Both MPH and (pure) RE curves have their advantages and disadvantages, and which to use depends on the application in mind.

4. Canal surface blending using RE curves

Blending is one of the important operations used in Computer-Aided (Geometric) Design. Blending surfaces are necessary for rounding edges and corners or for smooth connections of given objects. In what follows, we will deal with the cases when canal surfaces are used for the construction of a smooth transition between input shapes. We recall that canal surfaces are defined as envelopes of one parameter families of spheres in 3-space.

Any canal surface with a rational spine curve (a set of all centres of moving generating spheres) and a rational radius function has a rational parametrisation, as proved in Peternell and Pottmann (1997), Landsmann et al. (2001). However, a crucial part of the parametrisation algorithm is decomposing a positive polynomial into a sum of two squares (SOS problem) over reals, which is symbolically unsolvable, in general. Hence, a special role in geometric modelling is played by canal surfaces for which it is possible to find their rational representation without the need to solve the SOS decomposition.

Rational canal surfaces given by two curves were investigated by Bastl et al. (2014). This study revealed that for a canal surface to be rational it is not required that its medial axis transform is rational; square roots are allowed in the radius function. Such canal surfaces are, in general, not PN and do not possess rational offsets. However, they are in the more general class of surfaces called PSN surfaces (Vršek and Lávička, 2014), i.e., surfaces with Pythagorean surface normals along rational curves.

PN surfaces were introduced due to their straightforward applicability in CAD/CAM as they guarantee that the surface representing the centres of the spherical milling cutter is rational (and thus it can be described via the NURBS formalism). Nevertheless, this requirement can be unnecessarily strong in some situations as the milling cutter does not follow the whole offset surface but only some precomputed trajectories on it. So we do not have to assume that the PN property is satisfied globally but only along some special "suitably" distributed curves (trajectories of the milling cutter) along which the unit normals of the surface are rational. And it holds that all canal surfaces given by MATs in the form $\overline{\mathbf{y}}(t) = \left(\mathbf{y}(t), \sqrt{R(t)}\right)$ are exactly surfaces of this type as they contain a 1-parameter family of circles along which the unit surface normals are always rational. RE curves can serve as a simple tool for finding rational parametrisations of blending canal surfaces without the need to apply the SOS decomposition.

A method for computing rational canal blending surfaces between two given (parts of) canal surfaces using MPH curves was studied by Bizzarri and Lávička (2013). We now present a simplified method based on RE curves. Consider (parts of) two canal surfaces $\mathcal{S}_i$ given by their medial axis transforms $\overline{\mathbf{m}}_i(t) \subset \mathbb{R}^{3,1}$, $t \in [0,1]$, $i \in \{0,1\}$. Constructing a C^1/G^1 blending canal surface between $\mathcal{S}_i$ can be transformed into the problem of interpolating the C^1/G^1 Hermite data in $\mathbb{R}^{3,1}$

$$\mathbf{p}_i^* = \overline{\mathbf{m}}_i(i) \quad \text{and} \quad \mathbf{t}_i^* = \overline{\mathbf{m}}_i'(i), \tag{22}$$

and computing the canal surface given by the resulting interpolant considered as the MAT of the surface.

The key step in computing a rational parametrisation of a canal surface is finding a rational curve $\mathbf{c}(t)$ on it. The surface parametrisation is then obtained by rotating this curve around the tangents of the rational spine curve $\mathbf{m}(t)$ in the form

$$\mathbf{s}(t,u) = \mathbf{m}(t) + \frac{(\varrho(u) + \mathbf{m}'(t)) \star (\mathbf{c}(t) - \mathbf{m}(t)) \star (\varrho(u) - \mathbf{m}'(t))}{(\varrho(u) + \mathbf{m}'(t)) \star (\varrho(u) - \mathbf{m}'(t))}, \tag{23}$$

where $\varrho(u)$ is a rational function, the scalars and vectors in the sums $\varrho(u) \pm \mathbf{m}'(t)$ are considered as quaternions, and $\star$ is the operation of quaternion multiplication

$$(a + \mathbf{a}) \star (b + \mathbf{b}) = ab - \mathbf{a} \cdot \mathbf{b} + a\mathbf{b} + b\mathbf{a} + \mathbf{a} \times \mathbf{b}; \tag{24}$$

see Bizzarri and Lávička (2013), Bizzarri et al. (2015) for more details. Any rational choice of $\varrho(u)$ yields a rational parametrisation of the canal surface. One can choose e.g. $\varrho(u) = u$ yielding a low rational degree of $\mathbf{s}(t,u)$ in u, or $\varrho(u) = 2u/(1-u^2)$ for a relatively uniform distribution of the t-parameter lines.

Therefore, we need to interpolate the data in (22) by a rational (spine) curve and find a rational curve on the sought-after canal surface. We show that using contour curves (Bizzarri and Lávička, 2013) allows us to employ the RE interpolation procedure described in Section 3.

We now describe the particular steps of the method, which is summarised in Algorithm 1 and illustrated in Fig. 3. We project the data (22) to the hyperplane $z = 0$ by omitting the third co-ordinate, which yields

$$\mathbf{p}_i = \left(p_i^1, p_i^2, p_i^4\right), \quad \mathbf{t}_i = \left(t_i^1, t_i^2, t_i^4\right), \tag{25}$$

Algorithm 1 Canal surface blending using RE curves.

INPUT: Two canal surfaces $\mathcal{S}_i$ given by their medial axis transforms $\overline{\mathbf{m}}_i(t)$, $t \in [0,1]$, $i \in \{0,1\}$.

1: Set Hermite data (22) and project them to the hyperplane $z = 0$; see (25).
2: Compute the points and the tangent vectors at the corresponding boundary curve; see (12) and (13).
3: Construct $\mathbf{x}(t)$ interpolating $\mathbf{q}_i$ and $\mathbf{v}_i$, $i = 0, 1$.
4: Compute medial axis $\mathbf{y}(t)$ corresponding to $\mathbf{x}(t)$: $\mathbf{y}(t) = \left(x_1 + x_2' f, x_2 - x_1' f\right)$, where $f(t)$ interpolates (16).
5: Lift $\mathbf{y}(t)$ and $\mathbf{x}(t)$ to $\mathbb{R}^3$ and obtain the rational spine and the contour curve $\mathbf{m}(t)$ and $\mathbf{c}(t)$, respectively.
6: Rotate $\mathbf{c}(t)$ around the tangents of $\mathbf{m}(t)$.

OUTPUT: A parametrisation $\mathbf{s}(t,u)$ of the blending surface between the given canal surfaces $\mathcal{S}_i$.

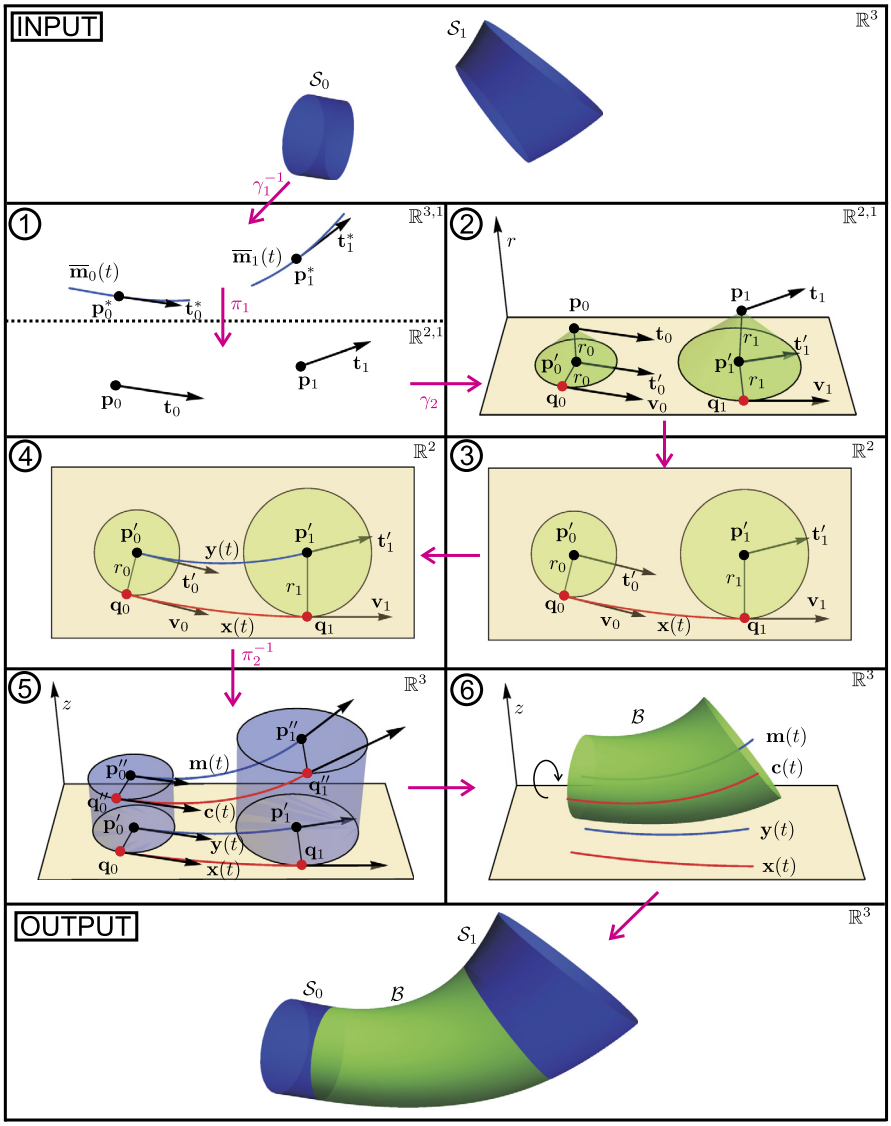

Fig. 3. An illustration of Algorithm 1 for canal surface blending using RE curves.

and consider these as data in $\mathbb{R}^{2,1}$. In turn, the data (25) are used as the input to the RE curve interpolation algorithm described in Section 3. This results in $\overline{\mathbf{y}}(t) \subset \mathbb{R}^{2,1}$.

In the last step, we lift $\overline{\mathbf{y}}(t)$ from $\mathbb{R}^{2,1}$ to $\mathbb{R}^{3,1}$. This is done by interpolating the one-dimensional data

$$p_i^3 \quad \text{and} \quad \beta_i t_i^3, \tag{26}$$

by a suitable function $g(t)$; β_is are of form (18). Again, we use the method of Ferguson. The sought-after MAT of the blending canal surface reads

$$\overline{\mathbf{m}}(t) = (y_1(t), y_2(t), g(t), y_3(t)), \qquad t \in [0,1]. \tag{27}$$

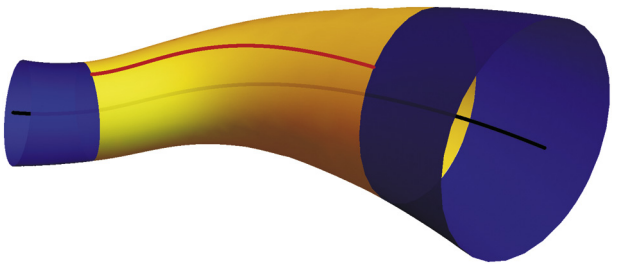

Fig. 4. A rational blending canal surface (yellow) with a rational contour curve (red) between the two canal surfaces (blue) from Example 4.1. (For interpretation of the references to colour in this figure legend, the reader is referred to the web version of this article.)

Additionally, the curve

$$\mathbf{c}(t) = (x_1(t), x_2(t), g(t)), \qquad t \in [0,1] \tag{28}$$

is, by construction, the rational contour curve of the constructed canal surface with respect to the vector $\mathbf{v} = (0,0,1)$.

Finally, by rotating the points of the contour curve $\mathbf{c}(t)$ around the tangents of the spine curve $\mathbf{m}(t)$, we arrive at the rational parametrisation $\mathbf{s}(t,u)$ of the blending canal surface; see the last part of Fig. 3.

Example 4.1. Consider two canal surfaces given by the respective MATs

$$\begin{aligned} \overline{\mathbf{m}}_0(t) &= \left(6t-6, t^2-2t+1, 3t^3-9t^2+9t-3, t^2-2t+2\right), \qquad t \in [0,1]; \\ \overline{\mathbf{m}}_1(t) &= \left(6t+6, t^2+2t+1, 3t^3+9t^2+9t+3, t^2+2t+2\right), \qquad t \in [0,1]. \end{aligned} \tag{29}$$

Using (22), we obtain the Hermite data

$$\mathbf{p}_0^* = (0,0,0,1), \quad \mathbf{p}_1^* = (6,1,3,2), \quad \mathbf{t}_0^* = (6,0,0,0), \quad \mathbf{t}_1^* = (6,2,9,2), \tag{30}$$

whose projection to the hyperplane $z = 0$ is

$$\mathbf{p}_0 = (0,0,1), \quad \mathbf{p}_1 = (6,1,2), \quad \mathbf{t}_0 = (6,0,0), \quad \mathbf{t}_1 = (6,2,2). \tag{31}$$

Computing boundary points and vectors via (12) and (13) yields

$$\mathbf{q}_0 = (0,1), \quad \mathbf{q}_1 = \left(\frac{24}{5}, \frac{13}{5}\right), \quad \mathbf{v}_0 = (4,0), \quad \mathbf{v}_1 = \left(\frac{32}{5}, \frac{24}{5}\right). \tag{32}$$

These data are then interpolated by the Ferguson cubic

$$\mathbf{x}(t) = \left(\frac{4}{5}\left(t^3+5t\right), \frac{1}{5}\left(8t^3+5\right)\right), \qquad t \in [0,1]. \tag{33}$$

Next, we compute the medial axis transform $\overline{\mathbf{y}}(t)$ in $\mathbb{R}^{2,1}$ corresponding to $\mathbf{x}(t)$; see (15). This leads to

$$\overline{\mathbf{y}}(t) = \left(\frac{2}{5}\left(t^5-t^4+2t^3+3t^2+10t\right), \frac{1}{15}\left(-3t^5+3t^4+19t^3-4t^2\right), \frac{\left(t^3-t^2+3\right)\sqrt{9t^4+6t^2+5}}{3\sqrt{5}}\right). \tag{34}$$

Lifting $\overline{\mathbf{y}}(t)$ to $\mathbb{R}^{3,1}$ is facilitated by interpolating (26) by the Ferguson cubic

$$g(t) = \frac{3}{5}\left(13t^3-8t^2\right). \tag{35}$$

Hence we obtain

$$\mathbf{m}(t) = \left(\frac{2}{5}\left(t^5-t^4+2t^3+3t^2+10t\right), \frac{1}{15}\left(-3t^5+3t^4+19t^3-4t^2\right), \frac{3}{5}\left(13t^3-8t^2\right)\right) \tag{36}$$

and

$$\mathbf{c}(t) = \left(\frac{4}{5}\left(t^3+5t\right), \frac{1}{5}\left(8t^3+5\right), \frac{3}{5}\left(13t^3-8t^2\right)\right). \tag{37}$$

Finally, rotating $\mathbf{c}(t)$ around the tangents of $\mathbf{m}(t)$, cf. (23), yields the rational PSN parametrisation (of rational degree $(11,8)$ in t and $(2,2)$ in s) of the blending canal surface (shown in Fig. 4).

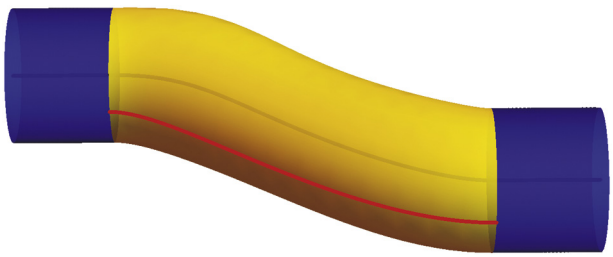

Fig. 5. A rational blending canal surface (yellow) with a rational contour curve (red) between the two cylinders (blue) from Example 4.2. (For interpretation of the references to colour in this figure legend, the reader is referred to the web version of this article.)

The following example presents an advantage of using RE curves in the blending process, when some standard methods fail; cf. Remark 3.3.

Example 4.2. Consider parts of two cylinders which are to be blended. They are represented by the Hermite data

$$\mathbf{p}_0^* = (0,1,0,1), \quad \mathbf{p}_1^* = (6,0,0,1), \quad \mathbf{t}_0^* = \mathbf{t}_1^* = (4,-3,0,0). \tag{38}$$

First, we project data (38) to the hyperplane $z=0$ and compute the associated boundary points and vectors in the form

$$\mathbf{q}_0 = \left(\frac{3}{5}, \frac{9}{5}\right), \quad \mathbf{q}_1 = \left(\frac{33}{5}, \frac{4}{5}\right), \quad \mathbf{v}_0 = \mathbf{v}_1 = \left(\frac{4}{5}, -\frac{3}{5}\right). \tag{39}$$

Following the presented contour blending method, the data of (39) are interpolated by the Ferguson cubic $\mathbf{x}(t)$, which is lifted to $\overline{\mathbf{y}}(t) \in \mathbb{R}^{2,1}$ and afterwards to $\overline{\mathbf{m}}(t) \in \mathbb{R}^{3,1}$, describing the canal blending surface with rational contour curve $\mathbf{c}(t) = (\mathbf{x}(t), m_3(t))$; see Fig. 5. Note that since $\mathbf{x}(t)$ is a cubic, the spine curve $\mathbf{m}(t)$ is a polynomial curve of degree 5 and the contour curve $\mathbf{c}(t)$ is a cubic.

It can be shown that when a standard approach based on PH and MPH curves is used (Kosinka and Lávička, 2011), a solution is not obtained for this input situation. In more detail, when RE curves are replaced by MPH curves then the interpolation by Ferguson cubic must be replaced by the interpolation using PH curves. Moreover when the same parametrisation degree of the resulting canal surface is required, one has to use G^1 interpolation by the PH (so called Tschirnhausen) cubic. However not all Hermite data can be interpolated by the PH cubic and this is exactly the case of the data of (39); see Kosinka and Jüttler (2006), Byrtus and Bastl (2010) for details on planar cubic PH interpolant existence.

One can still interpolate the data of (39) by PH curves of higher degrees. For instance, PH quintics (Farouki and Neff, 1995) always provide a solution, but this yields $\mathbf{m}(t)$ of degree 7 and $\mathbf{c}(t)$ of degree 5, which significantly raises the degree of the resulting blending surface.

We note that the presented method may not provide constant radii of the constructed blend when the input shapes are pipe surfaces with the same radii (e.g. cylinders), whereas the classical approaches based on interpolating data (38) and finding a rational curve (using SOS decomposition) on the corresponding canal surface have this feature. Nevertheless, we can use a suitable optimisation function such as

$$\chi(\alpha_0, \alpha_1) = \int_0^1 \left[r'(t, \alpha_0, \alpha_1)\right]^2 \mathrm{d}t \tag{40}$$

to obtain a 'pipe' surface of nearly constant radius. This optimisation was used in Fig. 5.

When constructing blending surfaces, we interpolate the input data in $\mathbb{R}^{2,1}$ by an RE curve. However, there is a two-parametric family of such interpolants; see Section 3. Thus, similarly to Example 3.2 and Fig. 2, we can choose desired shapes within this family. Two arbitrary chosen blending canal surfaces and two having optimised shapes are shown in Fig. 6.

5. Rational envelope surfaces

PN surfaces (Pottmann, 1995) are a natural generalisation of PH curves to the surface case. Similarly, MOS surfaces (Kosinka and Jüttler, 2007) represent a generalisation of MPH curves to the bivariate setting in $\mathbb{R}^{3,1}$. MOS surfaces correspond to associated domain boundaries which are rational via the envelope formula for a medial surface transform (MST), see Fig. 7. Although we are not aware of any direct applications as in the case of generalising MPH curves to RE curves, we lay down the basic concepts regarding RE surfaces as a generalisation of MOS surfaces.

For a C^1 segment $\overline{\mathbf{y}}(u,v) = (y_1(u,v), y_2(u,v), y_3(u,v), r(u,v)) \subset \mathbb{R}^{3,1}$ of an MST and its projection $\mathbf{y}(u,v) = (y_1(u,v), y_2(u,v), y_3(u,v)) \subset \mathbb{R}^3$, the corresponding boundary of the domain it represents is given by the envelope for-

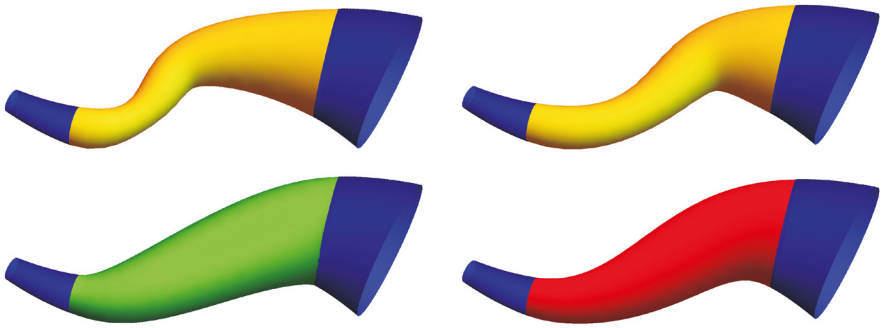

Fig. 6. Arbitrarily chosen rational blending canal surfaces (yellow), the rational blending surface corresponding to its RE curve with minimal arc-length (green) and minimal elastic blending energy (red) between two canal surfaces (blue). (For interpretation of the references to colour in this figure legend, the reader is referred to the web version of this article.)

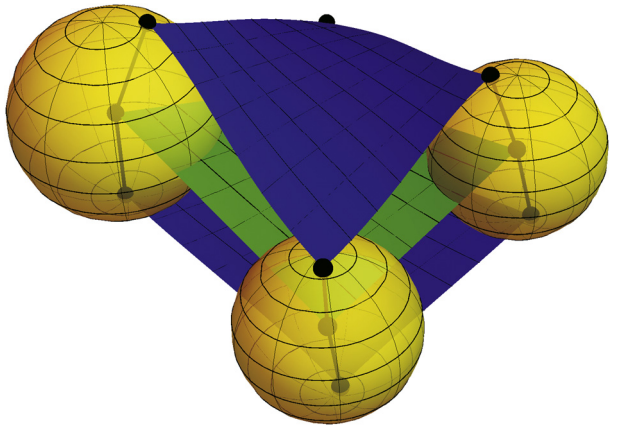

Fig. 7. The medial surface (green) and two branches (blue) of the envelope surface forming the boundary of a domain Ω. (For interpretation of the references to colour in this figure legend, the reader is referred to the web version of this article.)

mula

$$\mathbf{x}^{\pm} = \mathbf{y} - r\mathbf{n}_{\pm}, \tag{41}$$

where

$$\mathbf{n}^{\pm} = \frac{1}{EG - F^2}\left[\left(\frac{\partial r}{\partial u}G - \frac{\partial r}{\partial v}F\right)\mathbf{y}_u + \left(\frac{\partial r}{\partial v}E - \frac{\partial r}{\partial u}F\right)\mathbf{y}_v \mp \sqrt{\overline{EG} - \overline{F}^2}(\mathbf{y}_u \times \mathbf{y}_v)\right], \tag{42}$$

where $\mathbf{n}^{\pm}$ is a unit vector perpendicular to $\mathbf{x}^{\pm}$. The components $\overline{E}$, $\overline{F}$, $\overline{G}$ of the first fundamental form of $\overline{\mathbf{y}}(u, v)$ are computed using the indefinite Minkowski inner product with signature $(+, +, +, -)$ whereas the components E, F, G of the first fundamental form of $\mathbf{y}(u, v)$ are determined using the standard Euclidean inner product in $\mathbb{R}^3$. This envelope formula is a direct surface analogy to formula (1) for curves; see Kosinka and Jüttler (2007).

MOS surfaces are characterised by

$$\overline{EG} - \overline{F}^2 = \sigma^2(u, v), \tag{43}$$

where $\sigma(u, v) \in \mathbb{R}(u, v)$, which ensures that the envelope $\mathbf{x}^{\pm}$ is rational. Consequently, $\mathbf{x}^{\pm}$ possesses a normal vector field rationally parametrising the unit sphere, i.e., $\mathbf{x}^{\pm}$ are rational PN surfaces. Additionally, analogously to the univariate case, any rational MOS surface $\overline{\mathbf{y}}$ in $\mathbb{R}^{3,1}$ can be constructed starting from an (associated) rational PN surface $\mathbf{x}$ in $\mathbb{R}^3$ and a rational function r in the form

$$\mathbf{y}(u, v) = (x_1 + rn_1, x_2 + rn_2, x_3 + rn_3, r), \tag{44}$$

where $\mathbf{n} = (n_1, n_2, n_3) = (\mathbf{x}_u \times \mathbf{x}_v)/\|\mathbf{x}_u \times \mathbf{x}_v\|$.

However, MOS surfaces are not the only surfaces with rational envelopes. Turning back to (41), we only have to guarantee that $r\mathbf{n}^{\pm}$ is rational. This brings us to a broader class of (generally non-rational) *RE surfaces*, i.e., *surfaces yielding Rational Envelopes*. Accordingly, we set $r(u, v)$ as the square root of some non-negative function $R(u, v)$, which leads to

$$r\frac{\partial r}{\partial u} = \frac{1}{2}\frac{\partial R}{\partial u} \in \mathbb{R}(u, v), \quad r\frac{\partial r}{\partial v} = \frac{1}{2}\frac{\partial R}{\partial v} \in \mathbb{R}(u, v). \tag{45}$$

Then the rationality of $r\mathbf{n}^{\pm}$ (and thus also of the envelope $\mathbf{x}^{\pm}$), cf. (42), is guaranteed by the condition

$$R(\overline{EG} - \overline{F}^2) = \sigma^2(u, v). \tag{46}$$

Additionally, any RE surface $\overline{\mathbf{y}}$ in $\mathbb{R}^{3,1}$ can be constructed starting from an (associated) rational surface $\mathbf{x}$ in $\mathbb{R}^3$ and a rational function f in the form

$$\mathbf{y}(u, v) = (x_1 + f \cdot (\mathbf{x}_u \times \mathbf{x}_v)_1, x_2 + f \cdot (\mathbf{x}_u \times \mathbf{x}_v)_2, x_3 + f \cdot (\mathbf{x}_u \times \mathbf{x}_v)_3, f \cdot \|\mathbf{x}_u \times \mathbf{x}_v\|), \tag{47}$$

where $(\mathbf{x}_u \times \mathbf{x}_v)_i$ denotes the i-th coordinate of the cross-product. In contrast to MOS surfaces, it is now easy to generate RE surfaces in the form $(y_1, y_2, y_3, r^2 = R)$.

6. Conclusion

We have presented rational envelope curves as a generalisation of MPH curves. RE curves, although containing square roots, yield rational envelopes and can be constructed by simpler methods than those for MPH curves. To demonstrate the utility of RE curves, we proposed a simple interpolation algorithm for RE curves, which in turn can be used for canal surface blending using rational blends.

While the curve case with (M)PH and RE curves is well understood now, their surface analogies still pose many challenges. For instance, there are no direct algorithms for interpolation with PN surfaces, especially in the polynomial setting, which could then be utilised in the MOS case. On the one hand, rational envelope surfaces seem to avoid this limitation, but on the other hand, further research needs to be conducted in this area to place the bivariate case on the same firm footing as the univariate setting.

Acknowledgements

Michal Bizzarri and Miroslav Lávička were supported by the project LO1506 of the Czech Ministry of Education, Youth and Sports. We thank all referees for their valuable comments, which helped us to improve the paper.

References

Abhyankar, S., 1994. Square-root parametrization of plane curves. In: Bajaj, C. (Ed.), Algebraic Geometry and Its Applications. Springer, New York, pp. 19–84.
Bastl, B., Jüttler, B., Lávička, M., Schulz, T., Šír, Z., 2014. On the parameterization of rational ringed surfaces and rational canal surfaces. Math. Comput. Sci. 8 (2), 299–319.
Bizzarri, M., Lávička, M., Vršek, J., 2015. Canal surfaces with rational contour curves and blends bypassing the obstacles. Comput. Aided Des. 64, 55–67.
Bizzarri, M., Lávička, M., 2013. Parameterizing rational offset canal surfaces via rational contour curves. Comput. Aided Des. 45 (2), 342–350.
Blum, H., 1967. A transformation for extracting new descriptors of shape. In: Wathen-Dunn, W. (Ed.), Models for the Perception of Speech and Visual Form. MIT Press, pp. 362–380.
Byrtus, M., Bastl, B., 2010. G^1 Hermite interpolation by PH cubics revisited. Comput. Aided Geom. Des. 27, 622–630.
Choi, H., Lee, D., Moon, H., 2002. Clifford algebra, spin representation and rational parameterization of curves and surfaces. Adv. Comput. Math. 17, 5–48.
Choi, H.I., Han, C.Y., Moon, H.P., Roh, K.H., Wee, N.-S., 1999. Medial axis transform and offset curves by Minkowski Pythagorean hodograph curves. Comput. Aided Des. 31 (1), 59–72.
Farouki, R., 2002. Pythagorean-hodograph curves. In: Hoschek, J., Farin, G., Kim, M.-S. (Eds.), Handbook of Computer Aided Geometric Design. Elsevier, pp. 405–427.
Farouki, R., 2008. Pythagorean-Hodograph Curves: Algebra and Geometry Inseparable. Springer.
Farouki, R., Neff, C., 1995. Hermite interpolation by Pythagorean-hodograph quintics. Math. Comput. 64 (212), 1589–1609.
Farouki, R.T., 1996. The elastic bending energy of Pythagorean-hodograph curves. Comput. Aided Geom. Des. 13 (3), 227–241.
Hartshorne, R., 1977. Algebraic Geometry. Springer-Verlag.
Kosinka, J., Jüttler, B., 2006. G^1 Hermite interpolation by Minkowski Pythagorean hodograph cubics. Comput. Aided Geom. Des. 23, 401–418.
Kosinka, J., Jüttler, B., 2007. MOS surfaces: medial surface transforms with rational domain boundaries. In: The Mathematics of Surfaces XII. In: Lect. Notes Comput. Sci., vol. 4647. Springer, pp. 245–262.
Kosinka, J., Jüttler, B., 2009. C^1 Hermite interpolation by Pythagorean hodograph quintics in Minkowski space. Adv. Comput. Math. 30, 123–140.
Kosinka, J., Lávička, M., 2010. On rational Minkowski Pythagorean hodograph curves. Comput. Aided Geom. Des. 27 (7), 514–524.
Kosinka, J., Lávička, M., 2011. A unified Pythagorean hodograph approach to medial axis transform and offset approximation. J. Comput. Appl. Math. 235 (12), 3413–3424.
Kosinka, J., Šír, Z., 2010. C^2 Hermite interpolation by Minkowski Pythagorean hodograph curves and medial axis transform approximation. Comput. Aided Geom. Des. 27 (8), 631–643.
Landsmann, G., Schicho, J., Winkler, F., 2001. The parametrization of canal surfaces and the decomposition of polynomials into a sum of two squares. J. Symb. Comput. 32 (1–2), 119–132.
Moon, H., 1999. Minkowski Pythagorean hodographs. Comput. Aided Geom. Des. 16, 739–753.
Peternell, M., Pottmann, H., 1997. Computing rational parametrizations of canal surfaces. J. Symb. Comput. 23, 255–266.
Piegl, L., Tiller, W., 1997. The NURBS Book, 2nd edition. Monogr. Vis. Commun.. Springer-Verlag New York, Inc.
Pottmann, H., 1995. Rational curves and surfaces with rational offsets. Comput. Aided Geom. Des. 12 (2), 175–192.
Vršek, J., Lávička, M., 2014. Surfaces with Pythagorean normals along rational curves. Comput. Aided Geom. Des. 31 (7–8), 451–463.